CHEMISTRY
A EUROPEAN JOURNAL

DOI: 10.1002/chem.200701799

Understanding the Reactivity and Basicity of Zeolites: A Periodic DFT Study of the Disproportionation of N_2O_4 on Alkali-Cation-Exchanged Zeolite Y

Pierre Mignon,*[a] Evgeny A. Pidko,[b] Rutger A. Van Santen,[b] Paul Geerlings,[c] and Robert A. Schoonheydt*[a]

Abstract: The disproportionation of N_2O_4 into NO_3^- and NO^+ on Y zeolites has been studied through periodic DFT calculations to unravel 1) the role of metal cations and the framework oxygen atoms and 2) the relationship between the NO^+ stretching frequency and the basicity of zeolites. We have considered three situations: adsorption on site II cations with and without a cation at site III and adsorption on a site III cation. We observed that cations at sites II and III cooperate to stabilize N_2O_4 and that the presence of a cation at site III is necessary to allow the disproportionation reaction. The strength of the stabilization is due to the number of stabilizing interactions increasing with the size of the cation and to the Lewis acidity of the alkali cations, which increases as the size of the cations decreases. In the product, NO_3^- interacts mainly with the cations and NO^+ with the basic oxygen atoms of the tetrahedral aluminium through its nitrogen atom. As the cation size increases, the $NO_3^-\cdots$cation interaction increases. As a result, the negative charge of the framework is less well screened by the larger cations and the interaction between NO^+ and the basic oxygen atoms becomes stronger. NO^+ appears to be a good probe of zeolite basicity, in agreement with experimental observations.

Keywords: adsorption · basicity · density functional calculations · disproportionation · zeolites

Introduction

Zeolites are excellent acid–base catalysts. Acid zeolites are widely used in industrial catalysis both for their Brønsted (Al–OH–Si) and Lewis (extra-framework aluminium species) acidic properties. On the other hand, basic zeolites have generated interest because of their selectivity in catalysis[1–5] and their adsorption properties.[6,7] Their basicity is usually ascribed to the framework oxygen atoms in line with the general acid–base reaction shown in Scheme 1.

Scheme 1.

The basic oxygen of the zeolite is the oxygen atom that bridges the silicon and aluminium atoms. Oxygen basicity has been studied experimentally with probe molecules such as pyrrole,[8,9] CH_3OH and CH_3I,[10,11] and N_2O_4.[12,13] These studies led to two well-known empirical rules: 1) Basicity increases with the number of aluminium atoms in the lattice. 2) For a given amount of aluminium in the lattice, the basicity increases as the size of the exchangeable cation increases. Thus, the basicity sequence for the alkali cations is $[Li^+]$-Z < $[Na^+]$-Z < $[K^+]$-Z < $[Rb^+]$-Z < $[Cs^+]$-Z, in which Z refers to the zeolite.

In basic zeolites the exchangeable cations are Lewis acid centers. Therefore, any molecule in the zeolite can interact with the Lewis acid sites and with the framework oxygen atoms, which act as the basic sites. The separation of the two effects and their independence or cooperativity towards various processes is not straightforward. A better understanding of the role and interplay between these acidic and

[a] Dr. P. Mignon, Prof. Dr. R. A. Schoonheydt
Centrum voor Oppervlaktechemie en Katalyse
Katholieke Universiteit Leuven
Kasteelpark Arenberg, 23 B-3001 Leuven (Belgium)
Fax: (+32) 16-32-1593
E-mail: Pierre.Mignon@biw.kuleuven.be
Robert.Schoonheydt@biw.kuleuven.be

[b] Dr. E. A. Pidko, Prof. Dr. R. A. Van Santen
Schuit Institute of Catalysis, Eindhoven University of Technology
P.O. Box 513, NL 5600 MB Eindhoven (The Netherlands)

[c] Prof. Dr. P. Geerlings
Algemene Chemie, Vrije Universiteit Brussel
Pleinlaan 2, B-1050 Brussels (Belgium)

basic sites is a requisite for understanding the chemistry of cation-exchanged zeolites.

Several theoretical and experimental studies have been performed on cation-exchanged zeolites to characterize the acidic and basic sites. Experimentally, pyrrole is used as a probe molecule to measure the basicity of zeolites. The N–H group interacts with the framework oxygen and the resulting red shift of its stretching frequency is used as a measure of basicity.[8,9] In agreement with the above basicity trend, it was observed that the NH group is more strongly bound to the framework oxygen atoms in CsX than in LiX.[14] The adsorption of pyrrole on an MT_6 (T = Si or Al) cluster has been investigated theoretically by DFT methods for M = Li^+, Na^+, K^+, Rb^+, and Cs^+.[15] It was shown that the cation–π complex was the most stable. The cation hardness[16–18] was shown to be the driving force for the pyrrole adsorption. Indeed the heat of adsorption increases linearly with the electrostatic interaction between the cation and the π negative charge of the pyrrole ring.

Corrêa et al. investigated the elimination of a proton from ethyl chloride to form ethene on basic zeolite by performing DFT cluster calculations.[19] The activation barriers were found to increase from Li^+ to Cs^+. From the analysis of charges and geometries they concluded that the reaction is controlled by the Lewis acid–base interaction between the alkali cation (acid) and the chloride anion (base). Thus, the framework oxygen atoms are not involved in the process. Later Noronha et al. drew the same conclusion for the conversion of chloromethane into light olefins on cation exchanged ZSM-5.[20] The M–Cl electrostatic interaction, and thus, the interaction of the adsorbed molecule with the alkali metal cation, was shown to be the driving force for the formation of the methoxide.

On the other hand, it has been shown that the interaction with framework oxygen atoms can have a significant influence. The formation of methoxide from methanol and methyl iodide, two molecules possessing a hard (OH) and soft group (I), respectively, was again investigated. Experimentally, the chemisorbed methoxides were used as probes of the lattice oxygen basicity.[10,11,21] It was indeed observed that the ^{13}C MAS NMR spectroscopy chemical shift of the methoxy groups depends linearly on the Sanderson electronegativity[22] of a given zeolite structure. The theoretical investigation of these reactions using the ONIOM model showed two different trends for CH_3OH and CH_3I.[23] For CH_3OH the activation barriers increase from Li^+ to Cs^+, as was observed in the studies of Corrêa and Noronha.[19,20] For CH_3I the reverse trend was observed: The activation barrier decreases from Li^+ to Rb^+. The reason for this reverse trend is the soft character of the iodide. This leads to a weak interaction with the hard alkali cation. In this case the interaction between CH_3I and the basic oxygen atom prevails over the interaction with the alkali cation.

These studies showed that the lattice oxygen atoms and the exchangeable cations may have a different role with respect to the considered reaction. The basicity of the zeolite has also been studied experimentally with NO^+ as a probe molecule. The N_2O_4 disproportionation reaction generates nitrosonium (NO^+) and nitrate ions on the surface (Scheme 2). The nitrate is stabilized by the alkali metal and

Scheme 2.

the nitrosonium ion coordinates to the negatively charged lattice oxygen atoms. $\nu(NO^+)$ has been measured for both zeolites Y and X. Typically, an X faujasite-type zeolite is defined by a Si/Al ratio of 1.25. Zeolite Y has a typical Si/Al ratio of 2.4–2.5. For both, the NO^+ frequencies indicate that the order of basicity increases as follows: $[Li^+]$-Z < $[Na^+]$-Z < $[K^+]$-Z < $[Rb^+]$-Z < $[Cs^+]$-Z.[13] The $\nu(NO^+)$ frequencies are 15–50 cm^{-1} higher for zeolite Y than for zeolite X for any given cation, in agreement with the higher basicity of zeolite X.

The number and distribution of the cations over different sites of the framework may influence the adsorption and reaction processes. In faujasite zeolite, adsorption and reaction take place in the supercage. The cationic sites available for adsorption are sites II and III. Thus, in zeolite X the alkali cations occupy sites II and III. It has very recently been shown by periodic DFT calculations that these cations cooperate to stabilize NO_3^-, whereas the NO^+ cations interact with the lattice oxygen atoms.[24] In this study the computed NO^+ stretching frequencies were found to be in fair agreement with the experimental values.

In the present work we extended this study to zeolite Y exchanged with Na^+, K^+, and Rb^+. Because of the lower cation content of zeolite Y compared with X, site III has a lower probability of population, except for Rb^+; this cation is too large to enter the sodalite cages and hexagonal prisms.[25] Thus, in RbY, Na^+ cations occupy sites I and I′, whereas Rb^+ cations occupy sites II and III (see Figure 1). Several XRD studies on K^+-exchanged Y zeolites have shown that site II always contains a cation, but site III occupancy could not be demonstrated experimentally.[26] For NaY it has been shown by statistical models combined with XRD studies that for a typical Si/Al ratio of Y zeolite, no cations are present at site III.[27,28]

We have investigated in detail the role of alkali cations and framework oxygen atoms in the disproportionation of N_2O_4 on NaY, KY, and RbY. Three models were considered for each cationic form. Model SIIa corresponds to the adsorption of N_2O_4 on site II with one cation at site III. In model SIIb the adsorption occurs on site II without any cations at site III. And in model SIII N_2O_4 is adsorbed on site III. The adsorption of NO^+ on different sites and the corresponding NO^+ frequencies have also been computed and will be discussed in the context of zeolite basicity.

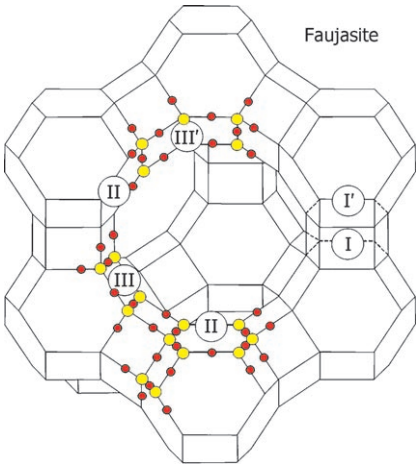

Figure 1. Structure of faujasite zeolite Y showing the location of sites I, I′, II, and III.

Methods and Model

Periodic density functional theory (DFT) as implemented in the Vienna Ab Initio Simulation Package[29,30] was used to compute equilibrium structures, their energies, and the vibrational frequencies of N_2O_4 adsorption complexes within alkali-exchanged zeolite Y. All calculations were performed by using the projected augmented waves (PAW) method to describe electron–ion interactions[31,32] and the Perdew–Wang (PW91) form of the generalized gradient approximation for the exchange and correlation energies.[33] Brillouin zone-sampling was restricted to the Γ point.[34] The kinetic energy cutoff was fixed at 400 eV. Full geometry optimizations were performed by using a conjugated gradient algorithm. Convergence was assumed to have been reached when the forces on each atom were below 0.05 eV Å^{-1}.

Vibrational frequencies of the adsorbed N_2O_4 species were calculated by using the finite difference method as implemented in VASP. Small displacements (0.02 Å) of atoms from the N_2O_4 species and zeolitic ions involved in direct interaction with N_2O_4 were used to estimate the numerical Hessian matrix. The rest of the zeolitic atoms were kept fixed at their equilibrium positions.

The adsorption energies of N_2O_4 and the disproportionation products in the zeolite were computed relative to the energy of the free zeolite and to the energy of N_2O_4 in a vacuum by using Equation (1).

$$\Delta E = E_{\text{complex}} - E_{0,\text{zeolite}} - E_{0,N_2O_4}$$

One drawback of DFT methods is that the dispersion interaction is not taken into account. Several recent studies have shown the importance of dispersion forces.[35,36] However, in our systems most of the interactions involve charged molecules and so are electrostatic in nature. Dispersion forces are thus assumed to have a minor influence on the trends resulting from our models.

A rhombohedral cell with 144 atoms (48 silicon and 96 oxygen) was used. Fourteen silicon atoms were substituted uniformly through the cell by aluminium atoms according to the Löwenstein rule to give a Si/Al ratio of 2.43 and a chemical composition of $M_{14}Al_{14}Si_{34}O_{96}$. Fourteen alkali cations were placed in the cell as follows: nine cations at site II, two at site I, two at site I′, and one at site III (Figure 1). For the model without any cation at site III (SIIb), the site III cation was moved to the corresponding site I′ site. Thus, there are nine cations at site II, two at site I, and three at site I′.

The cell parameters were first optimized in the absence of N_2O_4 for the three alkali cations (Table 1). These parameters were maintained for all of the other structures with adsorbed N_2O_4 and the disproportionation intermediates and products. The free N_2O_4 molecule was optimized in a $20\times20\times20$ Å^3 cell (Figure 2).

Table 1. Cell Parameters and metal–oxygen distances for cells containing Na^+, K^+, and Rb^+ cations.

	Cell lengths[a] [Å]	Cell angles[b] [°]
Na^+	17.57	60
K^+	17.72	60
Rb^+	17.80	60

[a] The cell lengths a, b, and c are equal, that is, $a=b=c$. [b] The cell angles α, β, and γ are equal, that is, $\alpha=\beta=\gamma$.

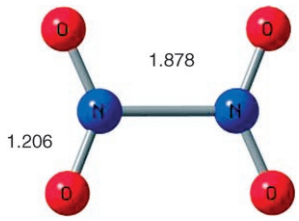

Figure 2. N_2O_4 geometry optimized in the $20\times20\times20$ Å^3 supercell with VASP.

From an XRD study of NaY zeolites, the SI–O3, SII–O2, SII–O4, SIII–O1, and SIII–O4 distances were determined to be around 2.69, 2.25, 2.93, 2.37, and 2.86 Å, respectively.[37] For KY, the SI–O3, SI′–O, SII–O, and SIII–O distances are in the ranges 2.53–2.97, 2.58–2.86, 2.69, and 2.89 Å, respectively.[38] These distances are in reasonably good agreement with our data (Table 2).

Table 2. Ranges of the metal–oxygen distances for cation sites I, I′, II, and III.

	Na^+	K^+	Rb^+
M(SI)–O3	2.36–2.62	2.80–2.93	2.85–3.14
M(SI′)–O	2.27–2.32	2.74–2.85	2.94–3.05
M(SII)–O2	2.27–2.39	2.71–2.89	2.83–3.12
M(SII)–O4	2.70–3.20	2.80–3.23	2.89–3.27
M(SIII)–O1	2.37–2.54	2.79–3.23	2.99–3.27
M(SIII)–O4	2.55–2.95	2.87–3.30	3.01–3.53

[a] Distances are given in Å. The number of the oxygen corresponds to the four types of oxygen atoms of the TOT bonds (tetrahedral–O–tetrahedral bonds).

To estimate the oxygen basicity, the electrostatic potential was computed for the free optimized zeolite structures to localize the most basic site as well as the values of the electrostatic potential in given locations. The electrostatic potential has already been successfully used to describe the basicity of oxygen atoms in previous cluster calculations.[23,39–41] For this purpose, high-precision single-point calculations were carried out on the optimized structures. The kinetic energy cutoff was augmented to 525 eV. Then the electrostatic potential map, projected over an isodensity surface (0.01 a.u.), was visualized by using the OpenDx software.[42] A homemade algorithm was used to locate the minimum of the electrostatic potential and to obtain the values at given locations.

Results

Three models have been considered. Model SIIa refers to the adsorption of N_2O_4 on a site II cation with a cation on

site III. Model SIIb corresponds to the adsorption on a site II cation without a cation on site III. In the SIII model, N_2O_4 is adsorbed on the site III cation. We call the primary interaction the interaction between N_2O_4 and the cation on which the molecule is adsorbed: a site II cation for the SII models and a site III cation for the SIII model. In the case of the SIIa model, secondary interactions arise with site II and III cations. For the SIIb and SIII models, secondary interactions involve only site II cations.

N_2O_4 adsorption: The geometries of the N_2O_4 adsorption complexes are shown in Figure 3 and the adsorption energies are given in Table 3. Upon adsorption in the supercage of zeolite Y, N_2O_4 interacts only with alkali cations. Oxygen atoms are not involved. This is indicative of a predominant $M^+\cdots N_2O_4$ electrostatic interaction. The adsorption of N_2O_4 leads to elongation of the N–O bonds and to shortening of the N–N bond compared with the gas-phase geometry (Figure 2).

The primary interactions, with the site II cations for the SII models and with the site III cation for the SIII model, constitute the major contribution to the stabilization of the adsorbed N_2O_4. For all of the models, the strength of the primary interaction decreases in the order $Na^+ > K^+ > Rb^+$, in accordance with the M^+–O distances. This is in line with the electrostatic field and Lewis acidity of the cations. The secondary interactions, between N_2O_4 and the other site II and III cations present in the supercage, increase in number and strength in the reverse order: $Na^+ < K^+ < Rb^+$ (see the distances in Figure 3). The contribution of the secondary interactions to the stabilization energy is the strongest for RbY, resulting in a better stabilization of the adsorbed N_2O_4.

Table 3. Adsorption energies [kJ mol^{-1}] of the adsorbed N_2O_4 molecule and the $[NO^{\delta+}\ ONO_2^{\delta-}]$ complex.

	Na^+	K^+	Rb^+
N_2O_4			
ΔE(SIIa)	−11	−11	−18
ΔE(SIIb)	−11	−10	−16
ΔE(SIII)	−33	−16	−29
$[NO^{\delta+}\ ONO_2^{\delta-}]$			
ΔE(SIIa)	25	−1	−14
ΔE(SIIb)	27	38	33

For the SII models with Na^+ and K^+, the secondary interactions are insignificant due to a large separation between N_2O_4 and the cations (large M^+–O distances). As a result, the stabilization energies are almost the same. For Rb^+ the secondary interactions exhibit M^+–O distances similar to those of the primary interactions. The strength of the secondary interaction is thus similar to the primary interactions. The larger number of secondary interactions for Rb^+ leads to better stabilization than with Na^+ and K^+ (Table 3).

For the SIIb model, without any cation at site III, the $M^+\cdots N_2O_4$ distances at site II are shorter by about 0.1 Å than those in the SIIa model. The primary interaction is thus reinforced. By comparing the energies of the SIIa and SIIb models, we can evaluate the effect of the site III cation, which is not present in the SIIb model. The effect is only noticeable for Rb^+ and is quite weak: The structure is 2 kJ mol^{-1} more stable in the presence of the site III cation.

For the SIII model, secondary interactions contribute actively to the stabilization of N_2O_4, whatever the alkali cation. The stabilization is consequently larger than that in the SII models. The N_2O_4 distances to the primary cation are all shorter in the SIII

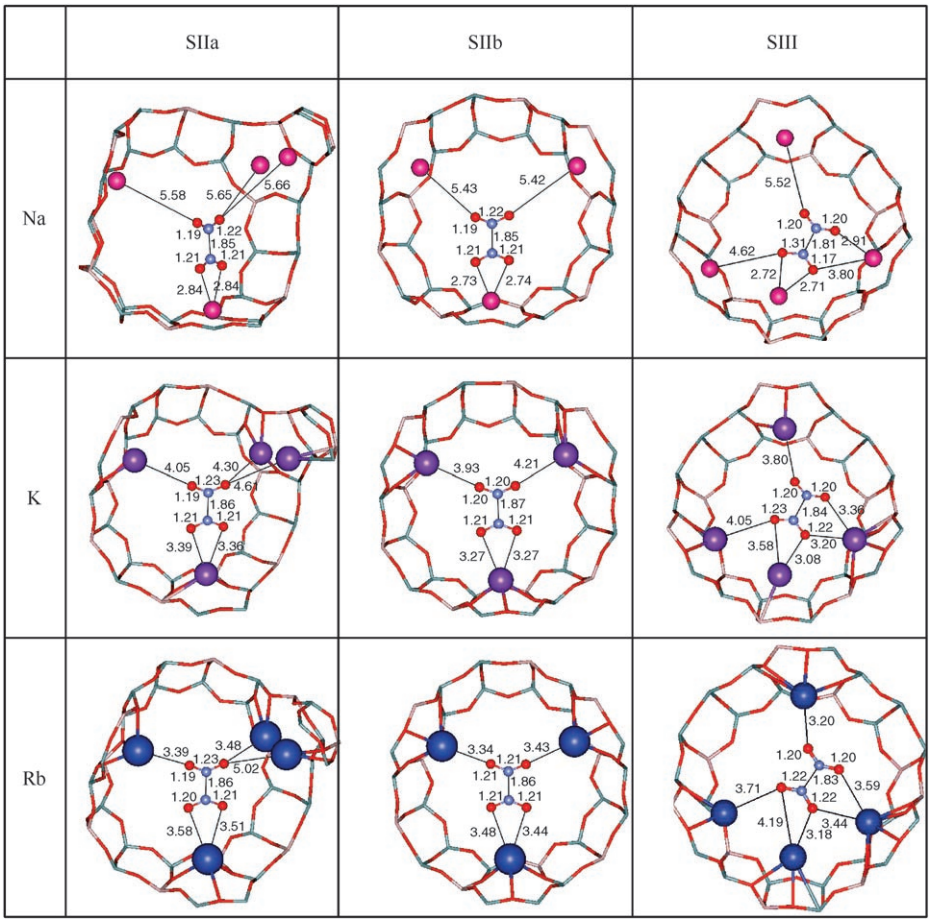

Figure 3. Geometries (distances in Å) of the N_2O_4-adsorbed molecule.

model than in the SIIa and SIIb models (Figure 3). This shows that the primary interaction of N_2O_4 with a site III cation is stronger in the SIII model than the primary interaction with a site II cation in the SII models. The effect of the site III cation is thus larger than that of the site II cation.

NaY provides a more stable complex in the SIII model than in the SII models. The interaction between N_2O_4 and the site III Na^+ cation is quite strong. The smallest distance observed between N_2O_4 and the alkali metal is 2.71 Å. Another strong secondary interaction arises with a site II cation (Na–O = 2.91 Å). With K^+ and Rb^+ the secondary interactions do not provide a better stabilization of N_2O_4. In the case of the adsorption of N_2O_4 on the site III Na^+ cation, the primary interaction and the Lewis acidity prevail over the effect of the multiple interactions in KY and RbY.

$ONONO_2$ adsorption: The $ONONO_2$ isomer consists of a $NO^{\delta+}$ part covalently bound by the nitrogen atom to one of the oxygen atoms of the $NO_3^{\delta-}$ moiety. This complex has already been characterized in the gas phase by QM calculations.[43] It is considered here to be an intermediate of the N_2O_4 disproportionation reaction before the separation of N_2O_4 into NO^+ and NO_3^-. The geometries of the adsorbed complexes are shown in Figure 4; the energies can be found in Table 3.

No reasonable geometries were found for the SIII model. The only geometry we were able to optimize shows two NO_2 radicals, which is incorrect for a closed-shell calculation; therefore, they are not considered herein. The fact that no geometry was found for an intermediate of the disproportionation reaction suggests that there is no stable structure of the $ON^{\delta+}$–$ONO_2^{\delta-}$ complex on the site III cation. The multiple interactions with the cations may directly lead to separation into NO_3^- and NO^+.

In the SII models, $NO^{\delta+}$ interacts with the surface oxygen atoms of the supercage and $NO_3^{\delta-}$ interacts with the alkali cations. For NaY, $NO_3^{\delta-}$ interacts only with the primary cations. For KY and RbY, secondary interactions increase in number and strength and result in a better stabilization, similar to the case of the N_2O_4 adsorption complex. In the SIIa model, the shortest distance between the $NO^{\delta+}$ moiety and the zeolite lattice oxygen atoms are 3.14, 3.03, and 2.80 Å for Na^+, K^+, and Rb^+, respectively. In SIIb they are 3.14, 2.80, and 2.88 Å, respectively (the distance for Rb^+ is not shown in Figure 4). The interactions between $NO^{\delta+}$ and the lattice oxygen, and between $NO_3^{\delta-}$ and the alkali cation, both increase with the size of the metal. As a consequence, $NO_3^{\delta-}$ and $NO^{\delta+}$ become increasingly separated in the series $Na^+ < K^+ < Rb^+$, as indicated by the distances between $NO^{\delta+}$ and $NO_3^{\delta-}$ of 1.77, 1.89, and 1.94 Å, respectively (Figure 4).

In the SIIb model, the structures are unstable (Table 3) due to the absence of the site III cation. This cation is necessary to stabilize $NO_3^{\delta-}$.

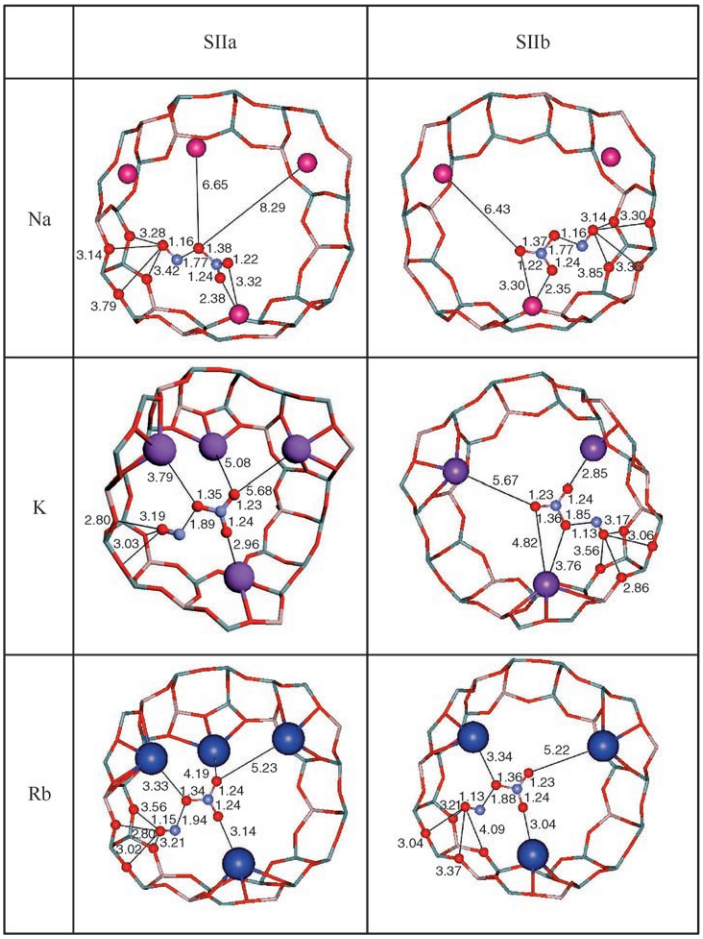

Figure 4. Geometries (distances in Å) of the $ON^{\delta+}$–$ONO_2^{\delta-}$-adsorbed isomer.

NO^+ and NO_3^- adsorption: The separated NO^+ and NO_3^- ion pair was optimized in the supercage of faujasite Y. NO_3^- interacts with the exchangeable cations, whereas NO^+ interacts with the negative framework oxygen atoms through the nitrogen atom. The three models, SIIa, SIIb, and SIII, refer to the adsorption of NO_3^- at sites II and III. In addition to these three models, we considered two possible configurations for the orientation of NO^+ and NO_3^-. In the SII models, NO^+ is in the same plane (first configuration) or orthogonal to NO_3^- (second configuration; see Figures 5 and 6, respectively). In the case of the SIII model, the difference lies in the coordination mode of NO^+. NO^+ is coordinated to two oxygen atoms in the first configuration and to four lattice oxygen atoms in the second configuration. The energies and NO^+ stretching frequencies are summarized in Table 4.

Structure stabilization: As seen above, the primary interactions decrease in the order $Na^+ > K^+ > Rb^+$. However, the strength and number of secondary interactions increases in the reverse order: $Na^+ < K^+ < Rb^+$. These multiple interactions lead to a better stabilization. Secondary interactions are naturally observed for adsorption on the site III cation

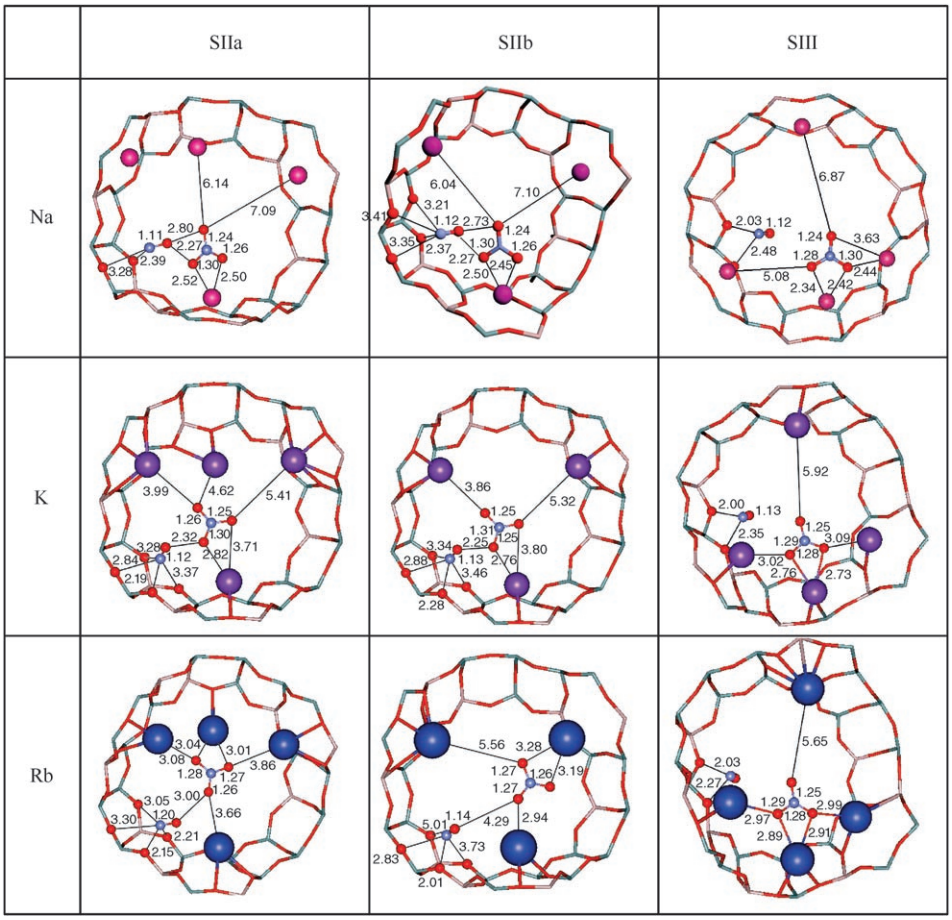

Figure 5. Geometries (distances in Å) of the NO^+- and NO_3^--adsorbed molecules in the first configuration.

because of the proximity of site II cations, whatever the alkali cation. As a result, stable structures are found for all cationic forms of the SIII model and for RbY in the SIIa model because of strong interactions between the NO_3^- moiety and the site III cation. The N_2O_4 disproportionation is thus only possible if an exchangeable cation is present at site III. This shows that the stabilization is driven by the $NO_3^-\cdots M^+$ interaction.

We can see that for all the cations in the two different configurations, the distances between NO_3^- and the site III cation are always shorter by about 0.1 Å than the NO_3^--site II cation distances. The interaction with the site III cation is stronger than the interaction with the site II cation due to less effective shielding of the site III cations by lattice oxygen atoms. Indeed, the site III alkali cation is coordinated to only four framework oxygen atoms instead of six for the site II cations. The efficiency of the shielding of the exchangeable cations has recently been shown to influence the stabilization of adsorbed molecules on low-silica zeolites modified with hard Lewis acids.[44,45] The importance of the site III cation can also be observed from the differences in the computed interaction energies between the SIIa and SIIb models with KY and RbY. The presence of the site III cation in SIIa leads to a greater stabilization: more than 70 kJ mol^{-1} in RbY (for both configurations).

NO^+–framework-oxygen interaction: In the first configuration of the SIIa model, the distance between NO^+ and the closest framework oxygen decreases from Na^+ (2.39 Å) to K^+ (2.19 Å) and Rb^+ (2.15 Å). For the SIII model the shortest distance varies only very slightly for Na^+, K^+, and Rb^+ (Δ= 0.03 Å; Figure 5). The distance from NO^+ to the second closest oxygen atom also decreases from Na^+ (2.48 Å) to K^+ (2.35 Å) and Rb^+ (2.27 Å). The same trend is observed for the SIIa model in the second configuration (Figure 6). For the SIII model the shortest distance from NO^+ to the closest framework oxygen is found for Rb^+ and there is a only a small difference between the Na^+ and K^+ structures (Δ= 0.03 Å). According to this data, the interaction between NO^+ and the framework oxygen atoms increases in the order $Na^+ < K^+ < Rb^+$.

The NO^+ stretching frequency (Table 4) decreases in the order $Na^+ > K^+ > Rb^+$ for all of the optimized structures (except for SIIb, second configuration). This also indicates an increasing interaction between NO^+ and the framework oxygen as the size of the alkali cation increases. These results are in agreement with the experimentally observed frequencies of 2090, 1973, and 1968 cm^{-1} for NaY, KY, and RbY, respectively.[13] The frequencies computed for the most stable structures, the SIII model and the first configuration, are close to those obtained experimentally.

In the case of the SII models we see that the planar orientation between NO^+ and NO_3^- (first configuration) is more stable than the orthogonal one (second configuration; see Table 4). In the SIII models the energy difference between the two configurations indicates that the coordination of NO^+ to two oxygen atoms (first configuration) leads to a better stabilization than in the four-coordinated mode (second configuration).

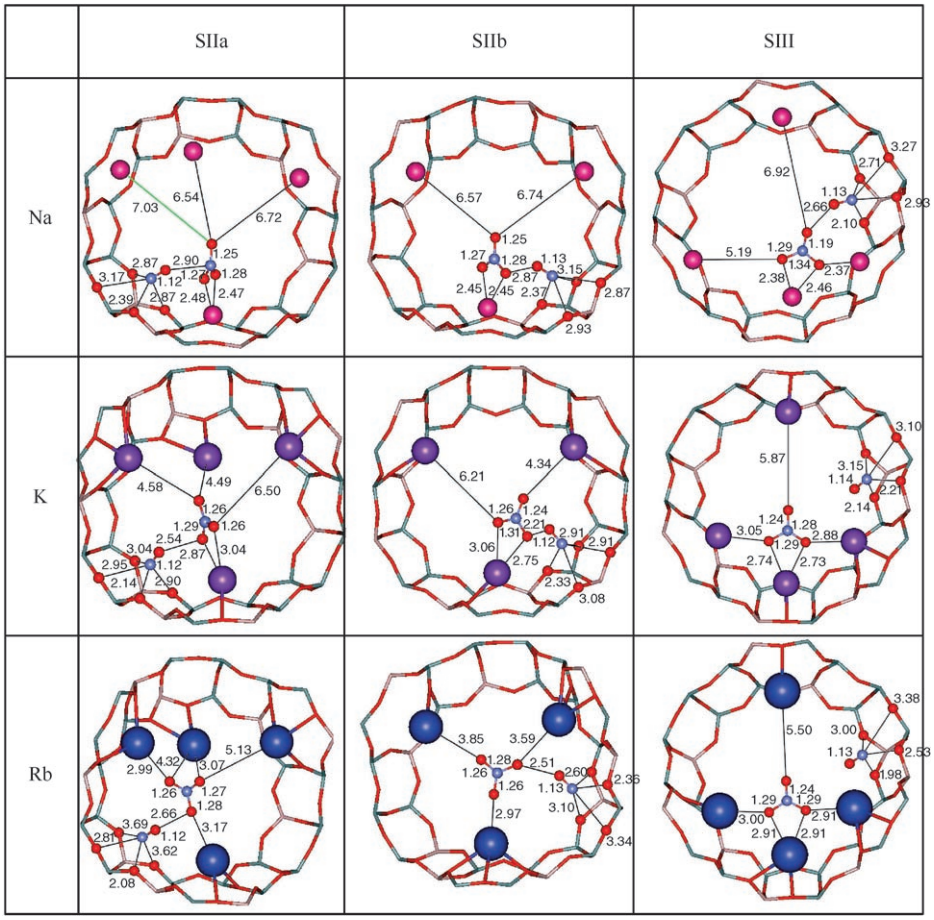

Figure 6. Geometries (distances in Å) of the NO^+- and NO_3^--adsorbed molecules in the second configuration.

Table 4. Adsorption energies [kJ mol^{-1}] and frequencies [cm^{-1}] of the adsorbed NO^+ and NO_3^- species.

		Na^+	K^+	Rb^+
1st configuration				
SIIa	ΔE	66	24	−25
	$\nu(NO^+)$	2045	2026	1964
SIIb	ΔE	62	63	47
	$\nu(NO^+)$	2050	2037	1950
SIII	ΔE	−30	−40	−50
	$\nu(NO^+)$	2007	1986	1967
2nd configuration				
SIIa	ΔE	107	46	−13
	$\nu(NO^+)$	2015	2009	2001
SIIb	ΔE	104	64	77
	$\nu(NO^+)$	1978	2038	2001
SIII	ΔE	−20	−16	−31
	$\nu(NO^+)$	2027	1961	1939

Discussion

In the disproportionation of N_2O_4 on cation-exchanged zeolites, both basic and acid sites are involved. The exchangeable cations are the Lewis acids, whereas the framework oxygen atoms are the basic sites. In previous studies, the reactivity of the alkali cations has been attributed to their Lewis acidity, which increases in the order $Cs^+ < Rb^+ < K^+ < Na^+ < Li^+$.[15,19,20] On the other hand, the basicity of the framework oxygen atoms has been shown experimentally to increase with the size of the exchangeable cations.[13] After N_2O_4 disproportionation, the characteristic vibrational frequencies of NO^+ and NO_3^- depend on the nature of the exchangeable cation. In particular, the NO^+ stretching frequencies are used to probe the basicity of the zeolites.[12]

Adsorption and disproportionation of N_2O_4: N_2O_4 adsorption in the zeolite Y supercage leads to stable structures. Only extra-framework cations are involved in the adsorption complex. The most stable structures are found when N_2O_4 is adsorbed on the site III cation. Stable structures corresponding to the intermediate $NO^{\delta+}ONO_2^{\delta-}$ could not be found for adsorption on the site III cation probably due to a strong interaction of $NO_3^{\delta-}$ with cations, which leads to direct separation into NO^+ and NO_3^-. After disproportionation, NO^+ and NO_3^- strongly interact with framework oxygen atoms and exchangeable alkali atoms, respectively. Stable structures are found only when NO_3^- is adsorbed on the site III cation. We conclude that the disproportionation of N_2O_4 into NO^+ and NO_3^- in the supercage of zeolite Y is feasible and exo-energetic only when a cation is present at site III.

The stabilization of N_2O_4 and the $[NO_3^- \; NO^+]$ complex is governed by the interaction with cations. The strength of the primary interactions parallels the Lewis acidity of the cations. Secondary interactions increase in number and strength with the size of the cation. The stronger the secondary interactions, the weaker the primary interactions become. In the case of K^+ and Rb^+, the sum of the two interactions results in an increase in the adsorption energies, which means that the secondary interactions dominate. In the case of Na^+, the strength of the primary interactions (Lewis acidity) is still dominant for the N_2O_4 adsorption and for the ion-pair adsorption with NO^+ in the second configuration. We conclude that both the Lewis acidity of the cations and the number of interactions with cations determine the overall stabilization. This contradicts previous theoretical studies which showed that the driving force of several reactions catalyzed by zeolites is the Lewis acidity of the exchangeable

cations.[19,20] One notes that these studies were performed by using cluster DFT calculations and therefore the influence of other exchangeable cations in the zeolite matrix were neglected.

The stronger interaction of N_2O_4 or NO_3^- with the site III cation than with the site II cation is due to two reasons: 1) Multiple interactions naturally arise upon adsorption on site III because of the proximity of the site III cation with the site II cations. For adsorption on site II, the SII models, the other site II cations in the supercage are too far away to stabilize the molecule. 2) The strength of the interaction with the site III cation is greater than with the site II cations. Indeed, a site III cation is more exposed in the supercage, it is less shielded by surface oxygen atoms, and it creates a stronger electrostatic field.[44] This was also observed in our study of zeolite X and confirms the dominant role played by the site III cation.[24]

Oxygen basicity: In the product structure, NO^+ interacts through its nitrogen atom with the lattice oxygen atoms, which carry the negative charge of the aluminium tetrahedron. The exchangeable cations interact both with lattice oxygen atoms and NO_3^-. One can note the interplay between NO_3^- stabilization by the cations and the NO^+ stabilization on lattice oxygen atoms. The stronger the cation···NO_3^- interaction, the weaker the cation···framework oxygen interaction becomes. The strength of the former interaction decreases in the order $Rb^+ > K^+ > Na^+$, whereas the reverse is valid for the latter: $Na^+ > K^+ > Rb^+$. This means that the negative charge of the framework oxygen atoms is less well screened in the case of Rb^+ than in the case of Na^+. As a result, the NO^+–framework-oxygen interaction is larger for larger cations. In other words, NO^+ interacts with more negatively charged oxygen atoms in the case of RbY than in the case of NaY. We conclude that the negatively charged framework oxygen atoms are more accessible in the case of large cations.

NO^+ is a 14-electron molecule with fully occupied π orbitals and empty π^* orbitals. Upon NO^+ adsorption some charge is transferred to the π^* orbital of NO^+. The N–O bond weakens and the corresponding stretching frequency decreases. The decrease observed in the NO^+ frequencies along with increasing cation size can therefore be related to the amount of charge transferred from the framework oxygen atoms. The amount of charge transfer is proportional to the amount of charge on the oxygen and thus proportional to the basicity. In conclusion, the basicity can be probed by the NO^+ frequency measurements.

The experimentally measured frequencies are 2090, 1973, and 1968 cm^{-1} for NaY, KY, and RbY, respectively.[13] In the most stable complexes with K^+ and Rb^+, that is, model SIII of the first configuration, the computed frequencies are close to the experimental ones. For Na^+ the difference between the experimental and computed values is large, 2090 and 2007 cm^{-1}, respectively. The value obtained experimentally for Na^+ (2090 cm^{-1}) was noted as being surprisingly large by Thibault-Starzyk et al.[13] They hypothesized that their NaY sample still contained traces of water, but this has to be verified by experiment. The value expected from a correlation between the frequencies and the hardness of the cations is 2020 cm^{-1}. This value is close to that determined in our calculations.

Theoretical assessment of oxygen basicity: Intrinsic basicity is defined as the density of negative charge on the framework oxygen atoms.[1] As mentioned above, all framework oxygen atoms carry negative charge and are potential basic sites. But only the oxygen atoms that acquire the highest negative charge have a true basic character and are considered to be basic sites. These are the oxygen atoms of the aluminium tetrahedron. Thus, the basicity will depend on the amount of aluminium substitution in the framework and on their distribution. It is an intrinsic property of the zeolite framework, irrespective of the nature of the cation.

Several theoretical calculations have been devoted to the evaluation of the negative charge of lattice oxygen atoms. Heidler et al.[7] computed the negative charge by using the electronegativity equalization method (EEM). They observed increasing negative charge on the oxygen with increasing cation size. The net atomic charge computed from various population analyses does not reproduce this trend.[23,40,46,47] On the other hand, the electrostatic potential (ESP) computed around a given atom is by definition the interaction between a positive charge and the electron density of the considered atom. It can be used to evaluate indirectly the negative charge carried by the atom. The ESP on cluster models of cation-exchanged zeolites has been shown to be a good descriptor of lattice oxygen basicity and successfully reproduces the effect of cation size on basicity.[23,40]

We have evaluated the basicity of two adsorption sites of NO^+ by computing the ESP on the corresponding lattice oxygen atoms of the SIII models. In the first configuration NO^+ is coordinated to two oxygen atoms (Figure 5); this is the most stable configuration. In the second configuration NO^+ is coordinated to four oxygen atoms (Figure 6). Table 5 shows the ESP values computed on the two- and four-fold NO^+ coordination sites computed by periodic calculations. The most negative values correspond to the largest basicity. The two-fold site shows the most negative ESP values. Thus, the two-fold site is more basic than the four-fold site. This leads to a better stabilization of NO^+, as can be seen by comparing the adsorption energies (Table 4). This can be explained by the distribution of the aluminium and the geometrical parameters. For the two-fold site, each

Table 5. Electrostatic potentials computed for the two- and four-fold sites.

	Electrostatic potential [kJ mol^{-1}]	
	Two-fold	Four-fold
Na^+	−627	−606
K^+	−589	−571
Rb^+	−595	−579

NO^+-coordinating oxygen atom is bound to an aluminium atom. For the four-fold site, only two of the four NO^+-coordinating oxygen atoms are bound to an aluminium atom. The distance between these oxygen atoms is smaller for the two-fold site (2.65, 2.67, and 2.69 Å for Na^+, K^+, and Rb^+, respectively) than for the four-fold site (3.90, 3.99, and 4.01 Å for Na^+, K^+, and Rb^+, respectively). Therefore, the interaction of NO^+ with the two oxygen atoms is stronger for the two-fold site. In comparison, for the four-fold site, NO^+ cannot interact as strongly with the two oxygen atoms of the aluminium tetrahedron because of the larger distances. The two-fold site is a more basic site.

In a topological study on the silicon/aluminium ordering in zeolite frameworks, Barthomeuf[48,49] studied the framework-induced basicity. The strength of the basic sites was evaluated with respect to the distribution of the AlO_4 tetrahedra and to the number of TOT bonds separating two AlO_4 tetrahedra. It was shown that the basicity of a given cluster decreases when more TOT bonds separate two AlO_4 tetrahedra. In our case, in the two-fold site the AlO_4 are separated by two TOT bonds: AlOSiOAlO. In the four-fold site the AlO_4 are separated by three TOT bonds: AlOSiOSiOAlO. According to these rules the two-fold site is more basic than the four-fold site, in agreement with the ESP calculations and the adsorption energies.

Note that the ESP values for Na^+ are overestimated compared with the values for K^+ and Rb^+. This may be due to the parameters we used for the pseudopotential of the alkali atoms. For each alkali cation the semicore p states were treated as valence states. In addition to the fact that the local pseudopotential was determined differently for Na^+ compared with K^+ and Rb^+, this leads to a large decrease in the energy cutoff from Na^+ to K^+. To increase the accuracy of the calculations with the PAW pseudopotential, the s states should be included in the valence states for K^+ and Rb^+. This is, however, the subject of a subsequent work on the evaluation of the electronic properties of atoms by using PAWs. On the other hand, the ESPs computed by cluster calculations reproduce well the basicity sequence: $Na^+ < K^+ < Rb^+$ (data not shown). In conclusion, the ESP is a good tool for evaluating the basicity of a given site in zeolites.

Comparison between zeolites X and Y: The NO^+ stretching frequencies obtained experimentally and computationally for zeolites X and Y are shown in Table 6. When NO^+ is adsorbed on a basic oxygen atom, electron transfer from the basic oxygen to the π^* orbitals of NO^+ occurs. The greater the electron transfer, the lower the NO^+ stretching frequency and the more basic is the oxygen atom. This is reflected well in the experimental NO^+ frequencies, which reveal that zeolite X is more basic than Y and that for both X and Y the basicity increases from Na^+ to K^+ to Rb^+. Thus, lattice oxygen atoms are more negatively charged and more basic when the cation size increases. The computed frequencies follow the expected trend with respect to the alkali cations.[24] However, the computed frequencies for zeolite X are all larger than those obtained for zeolite Y in disagreement with experimental results. The frequencies were calculated in exactly the same way in these two studies. So, this is unlikely to be the cause of the discrepancy.

Table 6. Adsorption energies and experimental and computed stretching frequencies of adsorbed NO^+.[a]

	Zeolite Y			Zeolite X		
	$\nu(NO^+)_{exptl}$ [cm^{-1}]	$\nu(NO^+)_{theory}$ [cm^{-1}]	ΔE [$kJ\,mol^{-1}$]	$\nu(NO^+)_{exptl}$ [cm^{-1}]	$\nu(NO^+)_{theory}$ [cm^{-1}]	ΔE [$kJ\,mol^{-1}$]
Na^+	2090	2007	−30	1976	2023	−69
K^+	1973	1986	−40	1927	1991	−91
Rb^+	1968	1967	−50	1903	1991	−82

[a] Experimental frequencies are taken from refs. [12,13], those computed for X zeolite are taken from ref. [24].

At a more fundamental level the differences between zeolites X and Y lie in the number of cations and aluminium tetrahedra per supercage. In our zeolite Y cell we have 14 aluminium tetrahedra and alkali cations, whereas the X cell comprises 22 aluminium and alkali metal ions. In zeolite Y there are four cations at site II and one at site III. In zeolite X there were four cations at each of the sites II and III. Another important factor is the distribution of the aluminium tetrahedral. A systematic study of the number and distribution of aluminium tetrahedra is necessary to see what the effect is on the NO^+ frequencies and on the basicity.

The adsorption energies of zeolite X (Table 6) are larger than those of zeolite Y because all the III sites contain a cation and the number of stabilizing interactions is higher. It was observed that secondary interactions dominate in all of the complexes and that the stabilization decreases in the order RbX > KX > NaX.[24] One exception was found for the separated complex [NO_3^- NO^+], for which the stabilization decreases in the sequence KX > RbX > NaX. K^+ has the same number of secondary interactions with NO_3^- as Rb^+, but a larger Lewis acidity (primary interaction). This is probably the reason for the sequence of the computed stabilization energies.

Conclusions

Our theoretical data on the disproportionation of N_2O_4 in the supercages of zeolites X[22] and Y reveal 1) the necessity to have an alkali cation at site III, 2) the cooperation between site II and III cations in the stabilization of NO_3^-, and 3) the competition between the number of interactions and the Lewis acidity of the cations. In addition, Na^+ is the smallest cation we have investigated and its Lewis acidity is the highest. However, not all Na^+ cations in the supercage can cooperate to stabilize NO_3^-; only two cations cooperate to stabilize NO_3^- in the adsorption on site III. The larger Rb^+ cations, which are not as strongly bound to sites II and III, all participate in NO_3^- stabilization. As a consequence, in the case of Na^+, NO^+ interacts with the supercage surface, the negative charge of which is partially screened by the Na^+ cations. The Rb^+ cations, on the other hand, are only slightly interacting with the surface oxygen atoms. The

$NO^+\cdots O$(surface) interaction is then maximal for Rb–Y-exchanged zeolites, and much lower in the case of Na–Y. This conclusion is also applicable to zeolite X. The experimentally observed increase in basicity in the series $Na^+ < K^+ < Rb^+$ can be ascribed to the above statements. It is based on the interplay of NO_3^- stabilization by cations, which increases with their size, and of the strength of the interaction between NO^+ and basic oxygen atoms, which also increases with the size of the cations.

The first consequence of our reasoning is that in the absence of site III cations the N_2O_4 disproportionation reaction cannot occur. In dehydrated zeolite Y, Na^+ and K^+ are not found at site III in XRD measurements.[26–28] However, N_2O_4 disproportionation was observed.[13] We postulate three reasons for this discrepancy: 1) small amounts of Na^+ and K^+, undetectable by powder XRD, are localized at site III, 2) the presence of N_2O_4 and its disproportionation products (NO^+ and NO_3^-) induces cation migration into site III, and 3) our model structure is not exactly identical to the experimental structures in terms of aluminium and alkali cation distribution. Clearly there is room for experimental research to find the minimum Si/Al ratio in faujasite-type zeolites at which N_2O_4 disproportionation will occur, that is, at which there are cations at site III.

Our study has highlighted the importance of the electric field of cations in zeolitic cavities and of the cooperative effect of these cations. These phenomena lead to the heterolytic dissociation of molecules such as N_2O_4, but also to the stabilization of charge-transfer states between two co-adsorbed molecules, such as olefins and O_2.[50] It might well be that ionic species are very important intermediates in base-catalyzed reactions in zeolitic cavities.

Acknowledgements

P.M. acknowledges a postdoctoral position at the KULeuven. This research was supported by the concerted research action of the Flemish government (GOA), by the scientific research communities (WOG) of the Flemish Fund for Scientific Research and by CECAT.

[1] D. Barthomeuf, *Catal. Rev. Sci. Eng.* **1996**, *38*, 521–612.
[2] A. Corma, *J. Catal.* **2003**, *216*, 298–312.
[3] R. J. Davis, *J. Catal.* **2003**, *216*, 396–405.
[4] H. Hattori, *Chem. Rev.* **1995**, *95*, 537–558.
[5] R. J. Venuto, *Adv. Catal.* **1968**, *18*, 331.
[6] C. P. Grey, D. R. Corbin, *J. Phys. Chem.* **1995**, *99*, 16821–16823.
[7] R. Heidler, G. O. A. Janssens, W. J. Mortier, R. A. Schoonheydt, *J. Phys. Chem.* **1996**, *100*, 19728–19734.
[8] M. Huang, S. Kaliaguine, *J. Chem. Soc., Faraday Trans.* **1992**, *88*, 751–758.
[9] D. Murphy, P. Massiani, R. Franck, D. Barthomeuf, *J. Phys. Chem.* **1996**, *100*, 6731–6738.
[10] V. Bosacek, *J. Phys. Chem.* **1993**, *97*, 10732–10737.
[11] V. Bosacek, S. Vratislav, M. Dlouha, *Collect. Czech. Chem. Commun.* **2004**, *69*, 1537–1552.
[12] O. Marie, N. Malicki, C. Pommier, P. Massiani, A. Vos, R. Schoonheydt, P. Geerlings, C. Henriques, F. Thibault-Starzyk, *Chem. Commun.* **2005**, 1049–1051.
[13] F. Thibault-Starzyk, O. Marie, N. Malicki, A. Vos, R. Schoonheydt, P. Geerlings, C. Henriques, C. Pommier, P. Massiani, *Stud. Surf. Sci. Catal.* **2005**, *158*, 663–670.
[14] S. Hashimoto, *Tetrahedron* **2000**, *56*, 6957–6963.
[15] R. J. Corrêa, *Tetrahedron Lett.* **2003**, *44*, 7299–7302.
[16] P. Geerlings, F. De Proft, W. Langenaeker, *Chem. Rev.* **2003**, *103*, 1793–1873.
[17] R. G. Parr, *Density Functional Theory of Atoms and Molecules*, Oxford University Press, New York, **1989**.
[18] R. G. Pearson, *Chemical Hardness*, Wiley-VCH, Weinheim, **1997**.
[19] R. J. Corrêa, E. F. Sousa-Aguiar, A. Ramirez-Solis, C. Zicovich-Wilson, C. J. A. Mota, *J. Phys. Chem. B* **2004**, *108*, 10658–10662.
[20] L. A. Noronha, E. F. Souza-Aguiar, C. J. A. Mota, *Catal. Today* **2005**, *101*, 9–13.
[21] V. Bosacek, R. Klik, F. Genoni, G. Spano, F. Rivetti, F. Figueras, *Magn. Reson. Chem.* **1999**, *37*, S135-S141.
[22] R. T. Sanderson, *J. Am. Chem. Soc.* **1983**, *105*, 2259–2261.
[23] P. Mignon, P. Geerlings, R. Schoonheydt, *J. Phys. Chem. B* **2006**, *110*, 24947–24954.
[24] E. A. Pidko, P. Mignon, P. Geerlings, R. A. Schoonheydt, R. A. van Santen, *J. Phys. Chem. C* **2008**, *112*, 5510–5519.
[25] G. L. Marra, *J. Phys. Chem. B* **1997**, *101*, 10653–10660.
[26] W. J. Mortier, H. J. Bosmans, J. B. Uytterhoeven, *J. Phys. Chem.* **1972**, *76*, 650–656.
[27] J. L. Lievens, W. J. Mortier, K. J. Chao, *J. Phys. Chem. Solids* **1992**, *53*, 1163–1169.
[28] J. J. Van Dun, K. Dhaeze, W. J. Mortier, *J. Phys. Chem.* **1988**, *92*, 6747–6754.
[29] G. Kresse, J. Furthmuller, *Comput. Mater. Sci.* **1996**, *6*, 15–50.
[30] G. Kresse, J. Hafner, *Phys. Rev. B* **1993**, *48*, 13115–13118.
[31] P. E. Blochl, O. Jepsen, O. K. Andersen, *Phys. Rev. B* **1994**, *49*, 16223–16233.
[32] G. Kresse, D. Joubert, *Phys. Rev. B* **1999**, *59*, 1758–1775.
[33] J. P. Perdew, J. A. Chevary, S. H. Vosko, K. A. Jackson, M. R. Pederson, D. J. Singh, C. Fiolhais, *Phys. Rev. B* **1992**, *46*, 6671–6687.
[34] H. J. Monkhorst, *Phys. Rev. B* **1976**, *13*, 5188–5192.
[35] C. Tuma, *Phys. Chem. Chem. Phys.* **2006**, *8*, 3955–3965.
[36] P. Ugliengo, *Chem. Phys. Lett.* **2002**, *366*, 683–690.
[37] J. A. Hriljac, *J. Solid State Chem.* **1993**, *106*, 66–72.
[38] W. T. Lim, S. Y. Choi, J. H. Choi, Y. H. Kim, N. H. Heo, K. Seff, *Microporous Mesoporous Mater.* **2006**, *92*, 234–242.
[39] P. Geerlings, A. M. Vos, R. A. Schoonheydt, *THEOCHEM* **2006**, *762*, 69–78.
[40] P. Mignon, P. Geerlings, R. Schoonheydt, *J. Phys. Chem. C* **2007**, *111*, 12376–12382.
[41] P. Mignon, S. Loverix, F. De Proft, P. Geerlings, *J. Phys. Chem. A* **2004**, *108*, 6038–6044.
[42] OpenDX. The Open Source SoftwareProject Based on IBM's Visualization Data Explorer, Version 4.4.0, **2006** (http://www.opendx.org/).
[43] M. L. McKee, *J. Am. Chem. Soc.* **1995**, *117*, 1629–1637.
[44] E. A. Pidko, R. A. van Santen, *ChemPhysChem* **2006**, *7*, 1657–1660.
[45] E. A. Pidko, J. Xu, B. L. Mojet, L. Lefferts, I. R. Subbotina, V. B. Kazansky, R. A. van Santen, *J. Phys. Chem. B* **2006**, *110*, 22618–22627.
[46] R. C. Deka, K. Hirao, *J. Mol. Catal. A: Chem.* **2002**, *181*, 275–282.
[47] R. C. Deka, R. Kinkar Roy, K. Hirao, *Chem. Phys. Lett.* **2004**, *389*, 186–190.
[48] D. Barthomeuf, *Microporous Mesoporous Mater.* **2003**, *66*, 1–14.
[49] D. Barthomeuf, *J. Phys. Chem. B* **2005**, *109*, 2047–2054.
[50] E. Pidko, R. A. van Santen, *J. Phys. Chem. B* **2006**, *110*, 2963–2967.

Received: November 15, 2007
Published online: April 25, 2008

